Mechanics & Industry **20**, 505 (2019)
© AFM, EDP Sciences 2019
https://doi.org/10.1051/meca/2019027

Mechanics & Industry

Available online at:
www.mechanics-industry.org

Regular Article

Effect of heat transfer on shear flow around an obstacle

Soumaya Hadj Salah[1,*], Mohamed Toumi[2], Walid Hassen[2], Habib Ben Aissia[2], and Jacques Jay[3]

[1] Research Unit of Ionized Backgrounds and Reagents Studies, University of Monastir, 5019 Kairouan Street, Monastir, Tunisia
[2] Research Unit of Metrology and Energy Systems, ENIM, University of Monastir, 5019 Kairouan Street, Monastir, Tunisia
[3] Thermal Centre of Lyon, National Institute of Applied Science of Lyon, 69621 Villeurbanne Cedex, France

Received: 26 March 2018 / Accepted: 22 March 2019

Abstract. The study of heat transfer on shear flows around an obstacle presents a great interest in determination of the influence of water on buildings and port infrastructures. The variation of the inlet temperatures and the influence of an obstacle placed at the bottom of a channel were analyzed. The obtained results supported by numerical simulations have shown that the doubling of the fluid inlet temperature significantly modifies all the dynamic characteristics of the shear flow. Pressure distribution, turbulent kinetic energy, dissipation rate, turbulent viscosity, and strain rate in the water channel were exposed. These results can help us to better exploit the flow of hot water discharged by power plants.

Keywords: Heat transfer / shear flow / turbulent kinetic energy / dissipation rate / turbulent viscosity / strain rate / inlet temperatures

1 Introduction

Cooling water discharged from power generation plants can cause several problems:
- Increase in seawater temperature. This will be a favorable factor for the extensive development of *Caulerpa taxifolia* that will be comforted by the warm waters and the destruction of some colony of *Posidonia*.
- The warming of bathing waters and its effect on tourist activities.
- The additional dilution of existing pollutants in the waters of the river.

So here we try to understand the shear flow around an obstacle at different temperatures for better use of water disposed from power plants.

In the study of properties of these flows, the use of simulation and numerical modeling has been very fruitful. Over the last few decades, the increase in the available means of calculation has allowed this type of flow to be successfully simulated numerically. Indeed, the understanding of physical processes that modify shear flow has been improved and many studies have been conducted to develop numerical shear models from appropriate perceptions. In a shear flow, the adjacent layers of the fluid move parallel to one another at different speeds. Viscous fluids [1] resist to this shearing motion. For a Newtonian fluid [2], the resistance applied by the fluid is proportional to the strain rate [3] or the shear rate [4]. Shear flow around an obstacle includes a variety of fluid dynamics phenomena, such as separation [5], stagnation [6], recirculation [7], fluctuations [8], and vortices [9]. The mechanisms of vortex formation [10] and its overpressure have significant effects on the different properties of the fluids. The combination of shear flow instabilities [11] and transient phenomena present in the boundary layers makes the numerical modeling of this flow very difficult.

In fact, the purpose of this article is to improve the understanding of the studied field by the specification of induced shear flows under the aerodynamic and hydrodynamic significant effects [12].

As far as we know, the study of heat transfer [13] effects on shear flows in the presence of obstacle was not sufficiently detailed numerically. Essentially, we want to show the influence of inlet temperatures on the perturbation of the shear flow. Practically we are trying to show numerically the change in the profile of the pressure distribution [14], as well as the turbulent kinetic energy [15] field, dissipation rate [16], turbulent viscosity [17], and strain rate. The first part of this article is devoted to a presentation of the physical model and different equations that control the shear flow. The second part deals with the validation of numerical model for fixed inlet temperatures with the experimental results of reference [18] and the numerical results of references [19,20]. The third part focuses on the obtained results and the interpretations for the different inlet temperatures [21].

* e-mail: Soumaya.hadj.salah@hotmail.fr

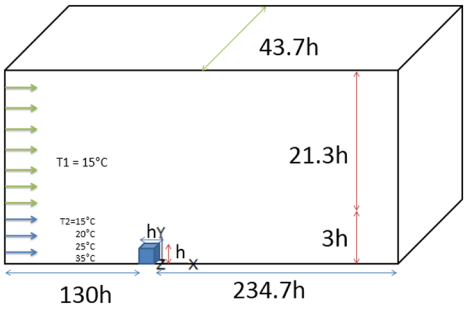

Fig. 1. Physical model of water channel.

2 Analyses

Sheared flows, which have great practical importance, are three-dimensional and time-dependent flows. Although researchers have successfully resolved differential equations [22] for fluid dynamics, even for time-dependent and three-dimensional flows, there is no universal model for shear flows that can be practically applied to all problems.

To model the shear flow, RANS techniques [23] were used with the modification of geometry and flow conditions. This solves the problem partially because most RANS models have been developed and calibrated free shear flow. The modifications aimed to correct certain deficiency of the model have been widely applied in nature. With this method, a procedure for calculating the temporal average [24] is used to represent the net effect of shear fluctuations without simulating the whole movement of unstable flow. However, the averaging process introduces unknown correlation terms that must be modeled.

2.1 Physical presentation problem

The physical presentation of the proposed problem is shown in Figure 1. We have used the same geometry of [20]. The temperature above the obstacle is constant ($T_1 = 15\,°C$), while that around the obstacle is variable ($T_2 = 15$, 20, 25, and 35 °C).

2.2 Mathematical model

The resolution of the hydrodynamics around an obstacle is based on the three-dimensional equations of Navier–Stokes (the conservation equations of mass and momentum). The dynamic viscosity is independent of strain rate and depends exclusively on the temperature and pressure; the shear flow with variable temperature is defined by the following equations.

Continuity equation:

$$\frac{\partial \rho}{\partial t} + \frac{\partial(\rho U_i)}{\partial x_i} = 0. \tag{1}$$

Momentum equation:

$$\frac{\partial(\rho U_i)}{\partial t} + \frac{\partial(\rho U_i U_j)}{\partial x_j} = -\frac{\partial P}{\partial x_i} + \frac{\partial}{\partial x_j}\left(\mu\left(\frac{\partial U_i}{\partial x_j} + \frac{\partial U_j}{\partial x_i}\right)\right) + F, \tag{2}$$

where F is the thermal buoyancy force $F = (F_i, F_j, F_k) = (0,\ \rho g\beta(T - T_0),\ 0)$.

Energy equation:

$$\rho C_p\left(\frac{\partial T}{\partial t} + U_i\frac{\partial T}{\partial x_i}\right) = \lambda\left(\frac{\partial^2 T}{\partial {x_j}^2} + \frac{\partial^2 T}{\partial {x_i}^2}\right). \tag{3}$$

We can simplify and apply the Reynolds rules to obtain the following averaged equations of continuity and momentum.

Averaged continuity equation:

$$\frac{\partial \overline{U_i}}{\partial xi} = 0. \tag{4}$$

Averaged momentum equation:

$$\overline{U_j}\frac{\partial\left(\rho\overline{U_i}\right)}{\partial x_j} = -\frac{1}{\rho}\frac{\partial p}{\partial x_i} + \left(\nu\frac{\partial^2\overline{U_i}}{\partial {x^2}_j}\right) + \frac{\partial\left(\overline{-\nu u_i^{\backprime} u_j^{\backprime}}\right)}{\partial x_j} + F. \tag{5}$$

The first term on the left represents the advection [25] of momentum; thereafter there is the term of the force due to the mean pressure field, and then the term of the motion distribution affected by shear and viscosity. The penultimate term is determined by the correlation ($u_i^{\backprime} u_j^{\backprime}$), between the turbulent fluctuations of velocity and the scalar quantity.

The K-ε standard turbulence model leads to the best agreement between the numerical results of reference [20] and the experimental results of reference [18] for the water channel. This model will be adapted in all the rest of work.

Averaged momentum equation:

$$\overline{U_i}\frac{\partial\overline{T}}{\partial x_i} = \alpha\left(\frac{\partial^2\overline{T}}{\partial {x_j}^2} + \frac{\partial^2\overline{T}}{\partial {x_i}^2}\right) + \frac{\partial\overline{(-\alpha T_i^{'})}}{\partial x_i}, \tag{6}$$

where $\alpha = \frac{\lambda}{\rho C_p}$.

2.2.1 Approximation of turbulent viscosity

The turbulent flow calculation methods, the temperature, and concentration fields are based, until now, on empirical hypotheses that try to establish a relationship between the Reynolds constraints [26] produced by the fluid motion and the average values of the velocity components, as well as the appropriate assumptions about heat and mass transfer [27].

$$\tau = \mu\frac{\partial u}{\partial y}, \tag{7}$$

where

τ is the shear stress,

μ is the dynamic viscosity,

u is the water velocity at a height y, and

y is the space coordinate identifying the fluid position.

Turbulent stresses [28] increase as the average rate of deformation increases [29]. Thus, the turbulent viscosity or the Boussinesq approximation [30] leads to a linear relationship between the shear stress and the turbulent

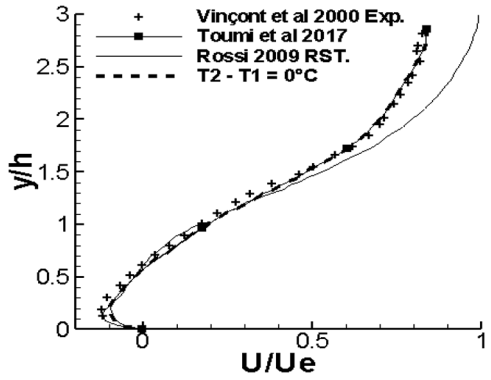

Fig. 2. Horizontal mean velocity field after the obstacle for $x = 4$ h at the bottom of a water channel.

strain rate given by

$$\tau_t = -\rho\overline{u_i u_j} = \mu_t\left[\frac{\partial(U_i)}{\partial x_j} + \frac{\partial(U_j)}{\partial x_i}\right] - \frac{2}{3}\left(\rho K + \mu_t\frac{\partial(U_i)}{\partial x_i}\right)\delta_{ij}, \quad (8)$$

$$\mu_t = C_\mu f_\mu \rho\frac{K^2}{\varepsilon}, \quad (9)$$

where

τ_t is the turbulent deformation rate,

μ_t is the turbulent viscosity,

C_μ is the specified empirical constant [31,32] (FLUENT UG. 2003) where the turbulent kinetic energy production is almost in equilibrium with the dissipation rate ($C_\mu = 0.09$),

f_μ is the damping function [31,32], (FLUENT UG. 2003)

K is the turbulent kinetic energy, and

ε is the dissipation rate.

It is well known that energy dissipation [33] and mass transport mechanisms [34] for laminar flow depend on the fluid viscosity. It is important to note that the laminar viscosity μ is a fluid property, unlike the turbulent viscosity μ_t, which is not a fluid property. Turbulent viscosity must be modeled to close the momentum RANS equation. The turbulent viscosity is determined by semiempirical formulas and replaced in the momentum equation RANS to obtain a solution.

2.2.2 Numerical validation

Figure 2 shows the variation of the horizontal velocity field in the water channel. The simulations were compared with experimental work [18] and numerical work [19,20]. A hybrid mesh of 336,793 nodes have been selected for the water channel; indeed, with these mesh numbers the error with respect to reference [18] does not exceed 1%.

3 Results and discussion

We show the influence of the presence of the obstacle as well as the change of inlet temperatures on the disturbance in the flow. For this, the following four cases were studied with different temperature values for the water channel:

Case 1: $T_e = T_1 = T_2 = 15\,°C$

Case 2: $T_e = T_1 = 15\,°C$, $T_2 = 20\,°C$

Case 3: $T_e = T_1 = 15\,°C$, $T_2 = 25\,°C$

Case 4: $T_e = T_1 = 15\,°C$, $T_2 = 35\,°C$

Our objective was to follow the influence of these inlet temperatures on changing of these settings: pressure distribution, turbulent kinetic energy, dissipation rate, turbulent viscosity, and strain rate in a water channel.

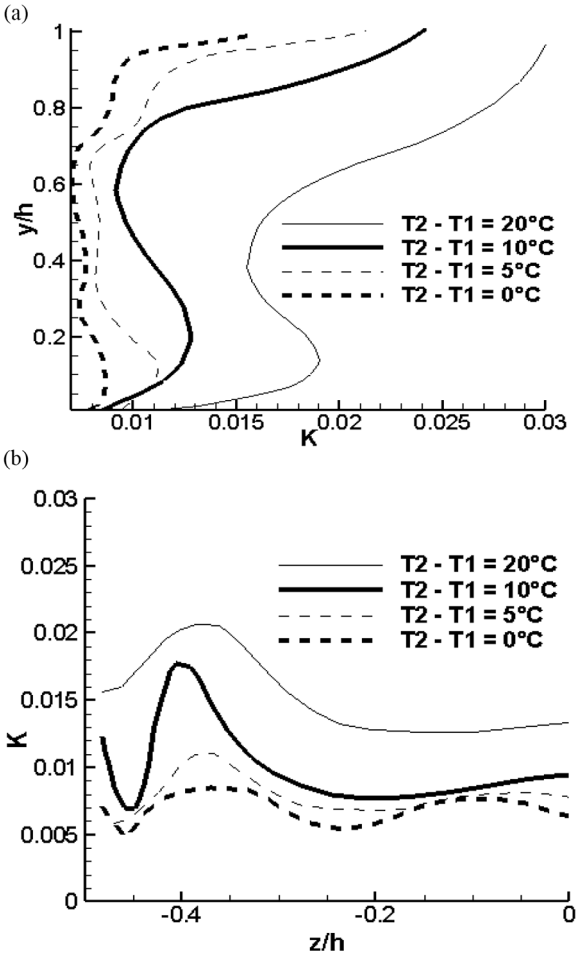

Fig. 3. Profile of the turbulent kinetic energy field after the obstacle for $x = 4$ h at the bottom of a water channel. (a) Horizontal. (b) Lateral.

3.1 Shear flow field for $T_2 = 15$, 20, 25, 35 °C when $T_e = T_1 = 15$ °C

3.1.1 Distribution of turbulent kinetic energy

Figure 3 shows the horizontal and lateral turbulent kinetic energy fields for the different inlet temperatures of abscissa $x = 4$ h after the obstacle at the bottom of the water channel. Maximum values of K are obtained near areas with a high temperature gradient, especially on the top of the obstacle. This is due to the production term in the K transport equation, which increases with temperature gradients and therefore intensify shear in the flux around

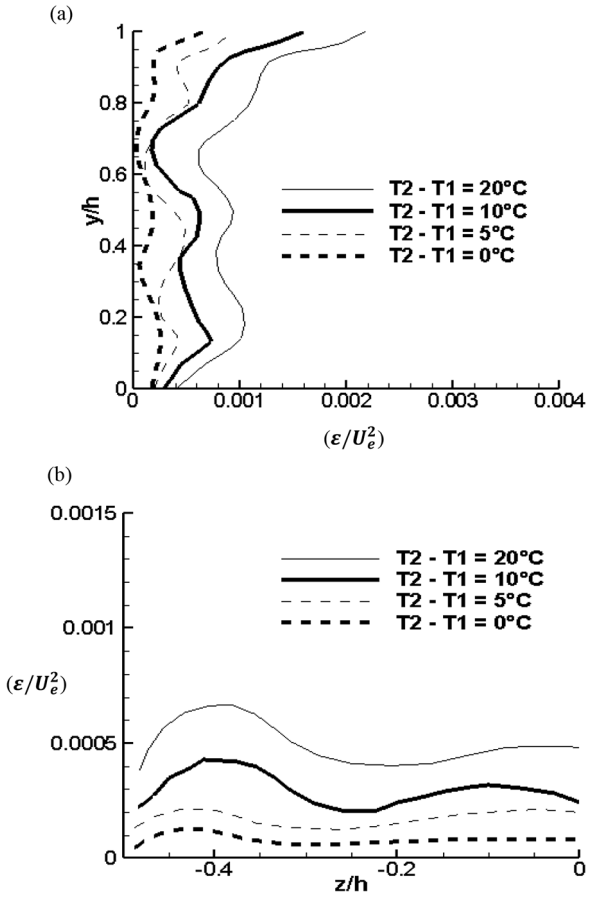

Fig. 4. Profile of dissipation rate after the obstacle for $x = 4$ h at the bottom of a water channel. (a) Horizontal. (b) Lateral.

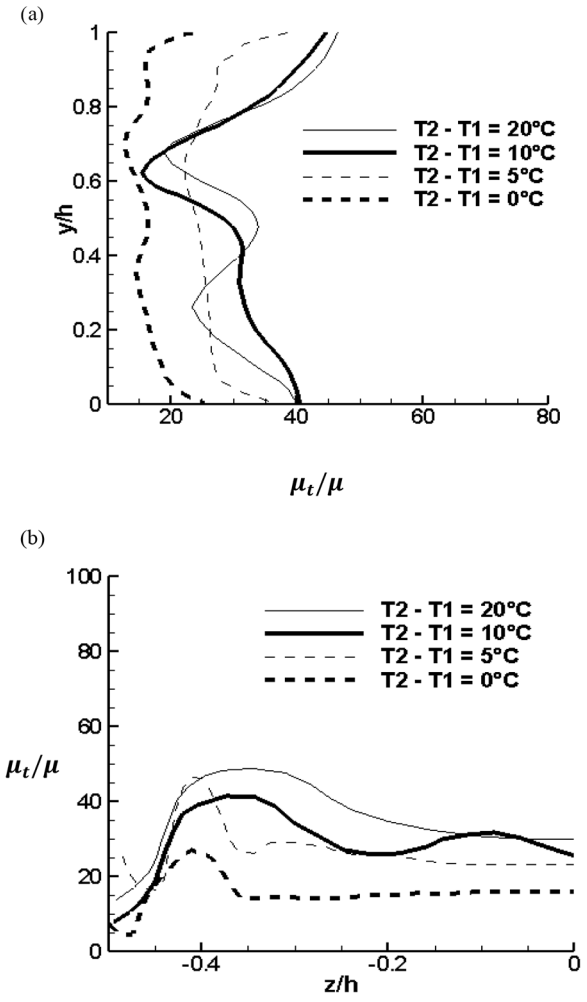

Fig. 5. Profile of turbulent viscosity after the obstacle for $x = 4$ h at the bottom of a water channel. (a) Horizontal. (b) Lateral.

this region. K values are almost zero at lower walls of domain. The horizontal and lateral turbulent kinetic energy are clearly intensified in the case of inlet temperature $T_2 - T_1 = 20\,°C$. The production of energy is affected over the obstacle to the interface of the two layers of increasing fluid temperature, where the shear is higher.

3.1.2 Components of dissipation rate field

The rate of energy dissipation is measured in terms of the dissipation rate of turbulence. This is an important parameter, which estimates the dissipated energy by the smallest vortex, and therefore the amount of energy when transferring the momentum to the domain walls. Figure 4 illustrates the profiles of the horizontal and lateral dissipation rate for the different inlet temperatures of the water channel: The balance between production and dissipation of turbulent kinetic energy is characteristic of RANS-based models.

From the curves, it is observed that the dissipation rate is high in regions with an important temperature gradient for $(T_2 - T_1 = 20\,°C)$ and low in regions with a low temperature gradient for $(T_2 - T_1 = 5\,°C,\ T_2 - T_1 = 0\,°C)$. Turbulent kinetic energy is transferred from biggest vortices to smallest vortices in the shear flow. The dissipation of lateral turbulence along the recirculation zone is much smaller than the horizontal dissipation rate distributions after the obstacle. These are higher due to the shear of the separated flow. The dissipation rate distribution indicates that the shear, in the lateral region, present a low amplitude relative to that of the recirculation zone after the obstacle. Thus, the smallest vortices dissipate the energy received. This energy dissipation is responsible of energy transfer in the shear flow.

3.1.3 Distribution of turbulent viscosity

Influenced by the values of K and ε, turbulent viscosity is defined as the resistance offered to the flow due to shear. The distribution of the turbulent kinematic viscosity μ_t dimensioned by the kinematic viscosity is shown in Figure 5. Interesting values of μ_t are determined near the edges of the obstacle under the flow. Note that the turbulent viscosity is directly proportional to K^2 and inversely proportional to ε. The viscosity estimates are much higher in the maximum pressure regions where the predicted value of K is high, whereas the dissipation is low. The imbalance between K and ε could be the reason for the abrupt transitions of the turbulent viscosity distribution in Figure 5. Similarly, the relationship between the turbulent viscosity and these two parameters is also indicated by low

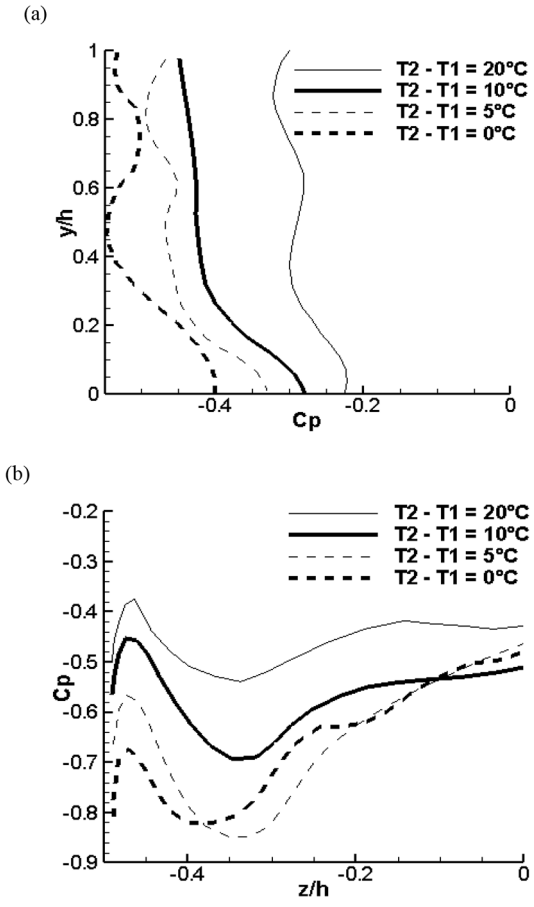

Fig. 6. Horizontal (a) and transversal (b) pressure coefficient distribution after the obstacle for $x = 4$ h at the bottom of a water channel.

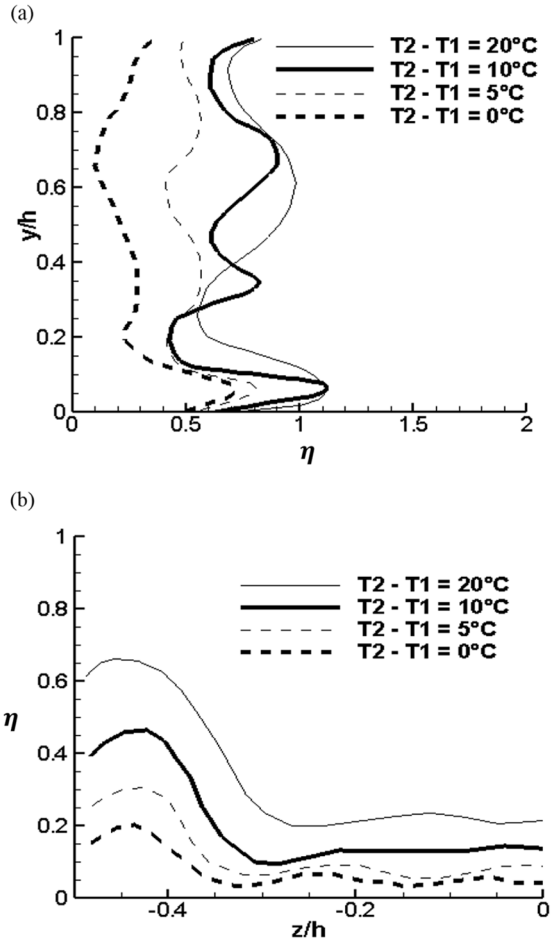

Fig. 7. Horizontal (a) and transversal (b) strain rate η distribution after the obstacle for $x = 4$ h at the bottom of a water channel.

horizontal values along the wake zone compared to the values of transverse turbulent viscosity. High values of horizontal turbulent viscosity are determined around the obstacle and in the recirculation zones near the bottom of the water channel. This is due to shear in these regions, having thus an almost increasing turbulent viscosity distribution from the bottom of the water channel to the upper limit of the obstacle. There is not a great intensification in the case of T_2–$T_1 = 20\,°\text{C}$ inlet temperature along the water channel because it is proportional to K^2 and inversely proportional to ε.

3.1.4 Pressure distribution on the surface of the obstacle

The surface pressure profiles for a cubic obstacle placed in a shear flow are studied by many researchers [35–37]. The pressure coefficient [38] is calculated as follows:

$$C_p = \frac{P - P_{\text{ref}}}{1/2\rho U_e^2}. \tag{10}$$

Here, the reference pressure P_{ref} is the static pressure at the lower limit of the domain calculated by the simulation code.

Figure 6 shows the pressure coefficient distribution at various inlet temperatures. The values of the pressure coefficients are completely negative due to the attachment after the obstacle and the selected reference pressure at the lower domain limit. For inlet temperatures $T_2 - T_1 = 20\,°\text{C}$, it is noted that the pressure recovery at the edges of all the lateral and horizontal surfaces of the obstacle is higher than the pressure coefficients for the other inlet temperatures, which are influenced by the separation region and the recirculation zone.

3.1.5 Strain rate distribution

The deformation rate S relates shear to viscosity. It is defined by

$$S_{ij} = \frac{1}{2}\left(\frac{\partial U_i}{\partial x_j} + \frac{\partial U_j}{\partial x_i}\right). \tag{11}$$

The dimensionless form of strain rate at the turbulent scale is given by

$$\eta = {}^{SK}/_{\varepsilon}. \tag{12}$$

This nondimensional parameter η is related to the anisotropic behavior [39] of the turbulent flow.

The distribution of the dimensionless parameter η with various input temperatures for an abscissa $x = 4$ h is shown

in Figure 7. Thus, it is obvious that the high temperature gradients in the flux induce greater deformation in the fluid. The deformation rate is maximal for $y/h = 0.5$, especially for the simulation of the shear flow with the inlet temperatures $T_2 - T_1 = 20\,°C$, where the deformation rate curve is continuous and increasing until the upper limit of the obstacle.

4 Conclusion

We presented the influence of variation of the input temperatures on the following parameters: pressure distribution, turbulent kinetic energy, dissipation rate, turbulent viscosity, and rate of deformation in a water channel. The results of the numerical simulations, presented in this work, have shown that the doubling of fluid inlet temperatures considerably increases all the dynamic characteristics of the sheared flow, hence the ability to capture the large-scale phenomena [40]. Also, energy production [41] is maximal above the obstacle until the shear interface for fluid layers with increasing inlet temperatures after the obstacle where the shear is very important.

The aim of this article is to explain the influence of inlet velocities on the parameters of shear flows. For the field of turbulent kinetic energy, the maximal energy values are obtained above the obstacle until the shear interface of the flow at inlet temperatures $T_2 - T_1 = 20\,°C$. For the field of vertical mean velocity, it was found that the region admitting both positive and negative values becomes wider for the inlet velocity $Ue_2 = 2\,Ue_1$ in comparison with the other inlet velocities. Therefore, this increase relates to the increase of the difference of the inlet velocities between the two fluids. The second variable to interpret is the dissipation rate: Maximal values of this parameter are obtained for the inlet temperature $T_2 - T_1 = 20\,°C$ at the top of the obstacle.

Shear simulations determined an increase of turbulent kinetic energies for high velocity gradient zones, as in the case of $T_2 - T_1 = 20\,°C$ inlet temperature. This amplification is balanced with the dissipation of turbulence, hence a good estimation of the turbulent viscosity. An increase of the pressure on the obstacle was obtained for $T_2 - T_1 = 20\,°C$ compared to the inlet temperatures $T_2 - T_1 = 10$, 5, and 0 °C.

Thus, the energy production will be greater at the upper limit of the obstacle where the shear is very important. Indeed, the high rate of deformation in this zone leads to, in proportion to the input velocities, a large production of energy and a large scalar dispersion. Therefore, the results of this study can be exploited to take better advantage of cooling water discharged by power plants for electricity production.

Nomenclature

C_p	Pressure coefficient
F	Force of obstacle per unit of volume (N/m^3)
H	height of the channel (m)
h	height of the obstacle (m)
K	Turbulent kinetic energy
L	length of the channel (m)
l	width of the channel (m)
P	Pressure (bar)
$\overline{P}$	Average pressure (bar)
p'	Pressure fluctuation
Reh	Reynolds number
Ue	Inlet velocity of the flow (m/s)
$\overline{U}$	Average velocity (m/s)
w'	Velocity fluctuation
S	Average deformation rate (s^{-1})
t	Dimensionless time
x,y,z	Cartesian coordinates

Greek letters

C_μ	Specified empirical constant
ε	Dissipation rate
f_μ	Damping function
μ	Dynamic viscosity ($kg/(m \cdot s)$)
ϑ	Kinematic viscosity (m^2/s)
ν_t	Turbulent kinematic viscosity
ρ	Density (kg/m^3)
σ_k	Prandtl number related to turbulent kinetic energy
σ_ε	Prandtl number related to dissipation rate
τ_t	Turbulent deformation rate
μ_t	Turbulent dynamic viscosity
η	Strain rate (s^{-1})

Superscripts

$'$	Dimensional variable

Subscripts

1, 2, 3 index of the Cartesian coefficient

References

[1] K. Hutter, Y. Wang, Viscous fluids, in: Fluid and Thermodynamics: Advances in Geophysical and Environmental Mechanics and Mathematics, Springer, Cham, 2016, pp. 347–421
[2] M. Jure, T. Primož, Laminar flow of a shear-thickening fluid in a 90° pipe bend, Fluid Dyn. Res. 38 (2006) 295–311
[3] T. George, High-strain-rate deformation: mechanical behavior and deformation substructures induced, Annu. Rev. Mater. Res. 42 (2012) 285–303
[4] H. Adrian, L. Martin, S. Jan, Finite element approximation of flow of fluids with shear-rate- and pressure-dependent viscosity, IMA J. Numer. Anal. 32 (2012) 1604–1634
[5] M. Jean, B. Vanden, Pouring flows with separation, Phys. Fluids 1 (1988) 156–171
[6] J. Kestin, R.T. Wood, On the stability of two-dimensional stagnation flow, J. Fluid Mech. 44 (2006) 461–479
[7] W.F. Robert, T.M. Alan, J.P. Philip, Introduction to fluid mechanics, 6th ed. John Wiley & Sons, Inc., New York, 2003
[8] H.L. Grant, B.A. Hughes, W.M. Vogel, A. Moilliet, The spectrum of temperature fluctuations in turbulent, J. Fluid Mech. 34 (2006) 423–442

[9] M. Fiebig, Vortices, generators and heat transfer, Chem. Eng. Res. Des. 76 (1998) 108–123
[10] B. Trung, S. Fotis, C. Dane, K. Daniel, Vortex formation and instability in the left ventricle, Phys. Fluids 24 (2012) 091110
[11] G.B. Peter, M.B. Humio, On the mechanism of shear flow instabilities, J. Fluid Mech. 276 (1994) 327–342
[12] Z. Shen, J. Niu, Y. Wang, H. Wang, X. Zhao, Hydrodynamic effects, in: Distribution and Transformation of Nutrients and Eutrophication in Large-Scale Lakes and Reservoirs, Advanced Topics in Science and Technology in China, Springer, Berlin, 2013
[13] Y.A. Cengel, A.J. Ghajar, Heat and mass transfer: fundamentals and applications, 4th ed. McGraw-Hill, New York, 2010
[14] K. Konrad, Z. Tadeusz, An analysis of pressure distribution in water and water emulsion in a front gap of a hydrostatic bearing, Teka Comm. Motor. Energetics Agric. 14 (2014) 45–52
[15] A.P. Koziol, Turbulent kinetic energy of water in a compound channel, Ann. Warsaw Univ. Life Sci. – SGGW Land Reclam. 43 (2011) 193–205
[16] M. Takeshi, L. Joon-Soo, S. Manabu, K. Sang-Hyun, P. Ig-Chan, Measurements of the turbulent energy dissipation rate ε and an evaluation of the dispersion process of the Changjiang diluted water in the East China Sea, https://doi.org/10.1029/2005JC003196
[17] J. Fe, L. Cueto-Felgueroso, F. Navarrina, J. Puertas, Numerical viscosity reduction in the resolution of the shallow water equations with turbulent term, Int. J. Numer. Methods Fluids 58 (2008) 781
[18] J.Y. Vinçont, S. Simoens, M. Ayrault, M. Wallace, Passive scalar dispersion in a turbulent boundary layer from a line source at the wall and downstream of an obstacle, J. Fluid Mech. 424 (2000) 127–167
[19] R. Rossi, G. Iaccarino, Numerical simulation of scalar dispersion downstream of a square obstacle using gradient-transport type models, J. Atmos. Environ. 43 (2009) 2518–2531
[20] M. Toumi, S. Haj Salah, W. Hassen, S. Marzouk, H. Ben Aissia, J. Jay, Three-dimensional study of parallel shear flow around an obstacle in water channel and air tunnel, Mechanics & Industry 18 (2017) 505–518
[21] M.N. Anton, Y.D. Anton, G.R. Vyacheslav, A.R. Vladimir, A.V. Elena, Assessment of allowable thermal load for a river reservoir subject to multi-source thermal discharge from operating and designed Beloyarsk NPP units (South Ural, Russian Federation), Environ. Model. Assess. 5 (2017) 1588–1595
[22] K. Kendricks, Interdisciplinary connections: applications of differential equations in water quality, biomechanics, and robotics, paper presented at the Annual Meeting of the Mathematical Association of America MathFest, Lexington Convention Center, Lexington, 2011, pp. 11–25
[23] W. Stephen, Coupling turbulence in hybrid LES-RANS techniques, J. Fluid Mech. 187 (2011) 61
[24] K. Igor, D.T. Lev, The space-time-averaging procedure and modeling of the RF discharge II. Model of collisional low-pressure RF discharge, IEEE Trans. Plasma Sci. 20 (1992) 66–75
[25] G.T. Velitchko, A.A. Alvaro, I.A. Felipe, Advection-dispersion-reaction modeling in water distribution networks, J. Water Resour. Planning Manage. 128 (2002) 334
[26] J.B. Maciej, H.D. Earl, R.N. Bernd, Low-dimensional modelling of high-Reynolds-number shear flows incorporating constraints from the Navier-Stokes equation, J. Fluid Mech. 729 (2013) 285–308
[27] K.W. Chen, H.T. Davis, E.A. Davis, G. Joan, Heat and mass transfer in water-laden sandstone: convective heating, Aiche J. 31 (1985) 1338–1348
[28] S.R. Martin, Measurements of the Reynolds stresses in a turbulent water flow and comparison with the [kappa-epsilon] computer model FLOW3D, AEA Technology 18, 1989
[29] H. Versteeg, W. Malalasekera, An introduction to computational fluid dynamics: the finite volume method, Pearson Education, 2007, pp. 43–49
[30] M. Paul, Stability, hyperbolicity and the Boussinesq approximation in layered shallow water, Atmosphere Ocean Science Colloquium, 2010
[31] FLUENT 6.1 User's Guide, Fluent Inc., Lebanon, 2003
[32] C. Fred, Aerodynamics for naval aviators workbook, Information Age Publishing Inc., Charlotte, NC, 1994
[33] V.P. Singh, M. Fiorentino, Entropy and energy dissipation in water resources, Kluwer Academic Publishers, Dordrecht, 1992
[34] F. Hugob, Mass transport mechanisms in partially stratified estuaries, J. Fluid Mech. 53 (2006) 671–687
[35] C. Senat, J.P. Guilhot, R. Gamba, Présentation d'un modèle de prévision des niveaux de pression dans les locaux encombrés, J. Phys. IV (1992) 471–484
[36] J. Sjah, E. Vincens, F. Leboeuf, M. Chaze, Modélisation 2D de l'écoulement visqueux autour d'un cylindre fixe par la méthode SPH-ALE 31èmes Rencontres de l'AUGC, E.N.S. Cachan, 2013
[37] Y. Eulalie, Étude aérodynamique et contrôle de la trainée sur un corps de ahmed culot droit, PhD thesis in Applied Mathematics and Scientific Calculation, University of Bourdeaux, France, 2014
[38] J.D. Anderson, Fundamentals of aerodynamic, 3rd ed., McGraw-Hill, 2001
[39] K. Kidena, Anisotropic diffusion of water in perfluorosulfonic acid membrane and hydrocarbon membranes, J. Membr. Sci. 323 (2008) 201–206.
[40] G.G. Cristóbal, S.G. Bernardo, E.L. Pérez-Lezama, The influence of large-scale phenomena on La Paz Bay hydrographic variability, Open J. Mar. Sci. 5 (2015) 146–157
[41] V.G. Fábio, M.R. Helena, R.R. Luisa, Energy production in water supply systems based on renewable sources, in: Environmental Hydraulics: Theoretical, Experimental and Computational Solutions, CRC Press, Boca Raton, FL, 2009, pp. 277–280

Cite this article as: S.H. Salah, M. Toumi, W. Hassen, H.B. Aissia, J. Jay, Effect of heat transfer on shear flow around an obstacle, Mechanics & Industry **20**, 505 (2019)